Volume 45 | Number 21 | 7 November 2016 | Pages 5797–6080

Chem Soc Rev

Chemical Society Reviews

www.rsc.org/chemsocrev

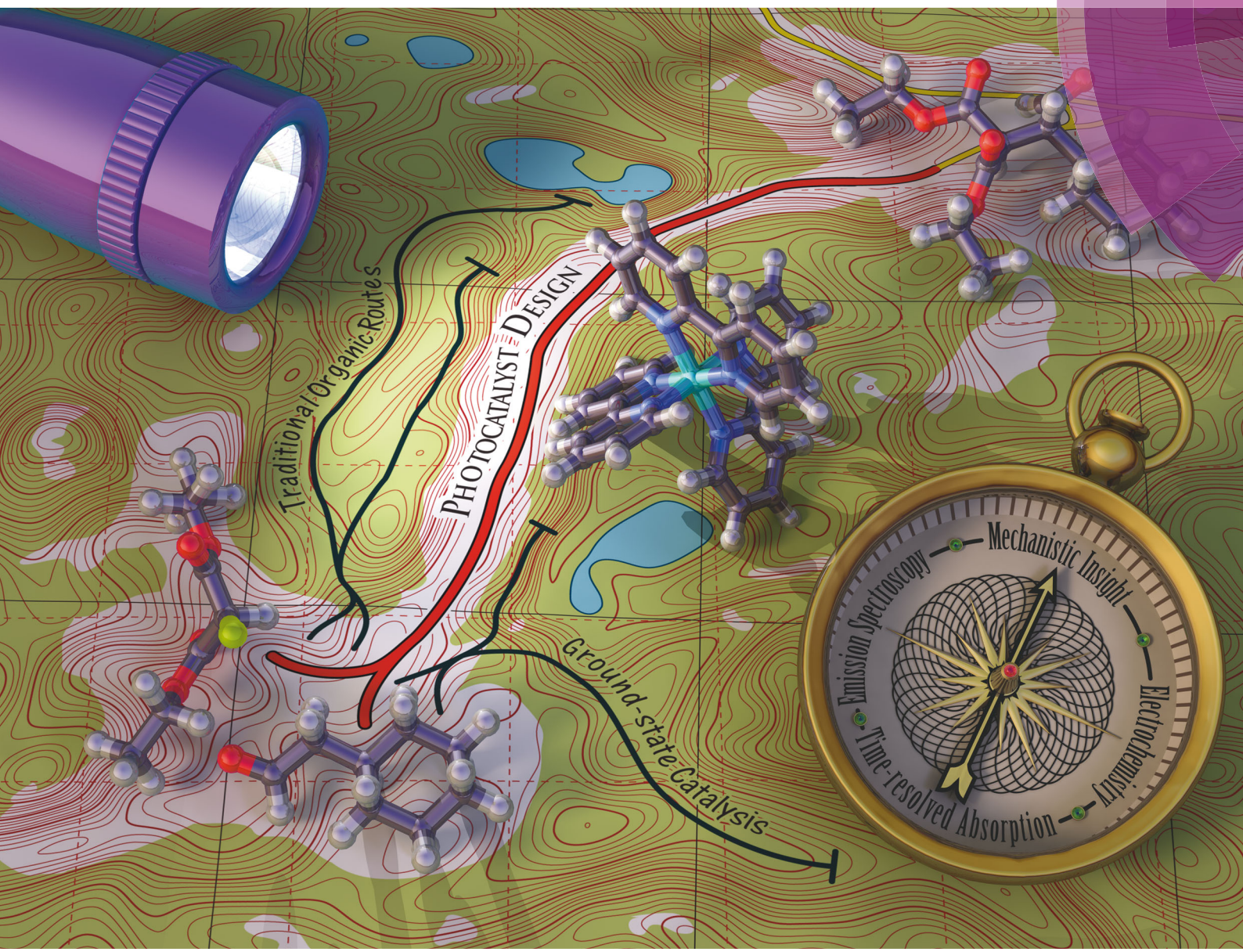

ISSN 0306-0012

ROYAL SOCIETY OF CHEMISTRY

TUTORIAL REVIEW

Daniela M. Arias-Rotondo and James K. McCusker

The photophysics of photoredox catalysis: a roadmap for catalyst design

175 YEARS

Chem Soc Rev

TUTORIAL REVIEW

View Article Online
View Journal | View Issue

Cite this: *Chem. Soc. Rev.*, 2016, **45**, 5803

The photophysics of photoredox catalysis: a roadmap for catalyst design

Daniela M. Arias-Rotondo and James K. McCusker*

Received 12th July 2016

DOI: 10.1039/c6cs00526h

www.rsc.org/chemsocrev

Recently, the use of transition metal based chromophores as photo-induced single-electron transfer reagents in synthetic organic chemistry has opened up a wealth of possibilities for reinventing known reactions as well as creating new pathways to previously unattainable products. The workhorses for these efforts have been polypyridyl complexes of Ru(II) and Ir(III), compounds whose photophysics have been studied for decades within the inorganic community but never extensively applied to problems of interest to organic chemists. While the nexus of synthetic organic and physical-inorganic chemistries holds promise for tremendous new opportunities in both areas, a deeper appreciation of the underlying principles governing the excited-state reactivity of these charge-transfer chromophores is needed. In this Tutorial Review, we present a basic overview of the photophysics of this class of compounds with the goal of explaining the concepts, ground- and excited-state properties, as well as experimental protocols necessary to probe the kinetics and mechanisms of photo-induced electron and/or energy transfer processes.

Key learning points

(1) The use of transition metal-based charge-transfer complexes as photo-activatable electron transfer reagents is beginning to play a significant role the field of catalytic organic chemistry.

(2) A deeper understanding of the fundamental concepts underpinning the field of inorganic photochemistry is critical to enable movement away from a "trial-and-error" approach for the selection of photocatalysts to one in which photocatalysts are designed and optimized for the reaction of interest.

(3) Stern–Volmer quenching studies, while useful for assessing whether a reaction between a substrate and a photo-active catalyst is occurring, must be supported by additional experiments in order to elucidate the mechanism(s) underlying photoredox catalysis.

(4) Many of the physical and photophysical properties that make transition metal charge-transfer complexes useful in photoredox catalysis can be replicated with organic chromophores, opening the door to new classes of photocatalysts that are metal-free.

(5) Combining the knowledge of photochemistry housed within that community with the chemical insight of synthetic organic chemists holds tremendous promise for transforming both fields, becoming more than the sum of its parts.

1. Introduction

The photophysics and photochemistry of transition-metal coordination compounds have been studied for many decades.[1–5] In particular, metal polypyridyl complexes – specifically those that possess visible charge-transfer absorption features – have played a central role in efforts to understand fundamental aspects of excited-state electronic structure and dynamics as well as the development of a wide range of solar energy conversion strategies.[2–5] The first report of $[Ru(bpy)_3]^{2+}$ (where bpy is 2,2′-bipyridine) acting as a photocatalyst was published in 1978.[6] There were a few reports employing both charge-transfer and organic chromophores as photocatalysts in the years that followed,[7,8] but photoredox catalysis as a vibrant field of synthetic organic chemistry can really be traced to 2008 with the simultaneous reports by MacMillan and co-workers[9] on the asymmetric alkylation of aldehydes photocatalyzed by $[Ru(bpy)_3]Cl_2$, and Yoon and co-workers[10] with the report of [2+2] enone cycloadditions, also using $[Ru(bpy)_3]Cl_2$. Following those initial reports, a growing number of research groups have explored the use of coordination compounds as photocatalysts for various organic transformations.[11] These compounds engage in single-electron transfer processes with organic substrates generating organic radicals, which play a major role in organic synthesis. This new kind of catalysis has opened the door to synthetically useful reactions that had previously been inaccessible.

As will be highlighted toward the end of this Tutorial, several groups have begun to shift their attention to the use of metal-free photoredox agents.[12] This important development notwithstanding, polypyridyl complexes of either Ru(II) or Ir(III) still comprise the majority of the photocatalysts currently employed.[11] The large number of examples in which $[Ru(bpy)_3]^{2+}$ has been

Department of Chemistry, Michigan State University, East Lansing, Michigan, 48824, USA. E-mail: jkm@chemistry.msu.edu

utilized might make this compound look like a "one size fits all" chromophore, when in reality, the best choice of photocatalyst for a given reaction is determined by the kinetics and thermodynamics of the system of interest. The challenge, of course, is that the measuring, understanding and ultimately manipulating physical and photophysical properties of these chromophores has by and large been the domain of the inorganic community, whereas the knowledge and insight into what chemical transformations are potentially interesting lie within the synthetic organic community. The purpose of this Tutorial is, in part, to help bridge this gap. In this regard, this Tutorial is not designed to be a review of the field of photoredox catalysis, but rather to present an overview of certain aspects of inorganic photophysics (both conceptual as well as in terms of experimental protocol) that are most relevant for their application to problems in photoredox catalysis. Given the widespread use of $[Ru(bpy)_3]^{2+}$ in this chemistry we will use this molecule as a template for the discussion, but it is important to note that the concepts that will be discussed can be applied (with some modifications) to most transition-metal photocatalysts as well as metal-free photoredox catalysts.

2. Photoredox catalysts: a wishlist

The field of photochemistry is rather broad, encompassing a range of processes including electron and energy transfer, isomerization and ligand substitution to name a few. Photoredox catalysis primarily deals with electron transfer processes that are initiated by the absorption of a photon by a chromophore (*i.e.*, the photocatalyst). Such systems take advantage of the enhanced redox reactivity of the chromophore in its excited state to facilitate a reaction that would not proceed otherwise; in this sense, light provides the added energy needed to make the reaction thermodynamically viable. Although there have been reports of reactions driven by photo-induced energy transfer,[11] the majority of the work in this area centers around photo-induced electron transfer processes utilizing charge-transfer chromophores like $[Ru(bpy)_3]^{2+}$; being able to experimentally differentiate between electron and energy transfer processes is an important issue from a mechanistic perspective and will be discussed in detail in this Tutorial, but the chemical focus will remain primarily on photoredox (*i.e.*, electron transfer) reactions.

In any photocatalytic cycle, the key step is the absorption of a photon that leads to the formation of an excited state that then engages in a chemical reaction. Scheme 1 shows two examples of photoredox catalytic cycles involving a Ru(II) chromophore; the one on the left, reported by Zheng and co-workers,[13] uses $[Ru(bpz)_3]^{2+}$ (where bpz is 2,2′-bipyrazine) and is called reductive because the excited photocatalyst accepts an electron from another molecule. The cycle on the right, reported by Cano-Yelo and Deronzier[14] is an oxidative cycle, *i.e.*, the excited state of the photocatalyst is first oxidized and then reduced to reform its resting state.

Most steps in a photoredox catalytic cycle are bimolecular reactions and can be represented as shown in Scheme 2.[2,15] The first step is the absorption of a visible light photon by the photocatalyst in its ground state (PC) and its consequent promotion to an electronic excited state (PC*); k_0 represents the rate of excited-state relaxation (in this case ground-state recovery). This process can be radiative (*i.e.*, emission) and/or non-radiative and will be discussed in detail in the Excited-state kinetics section. For the excited photocatalyst to react with a molecule (M), both species must diffuse towards each other, forming a "precursor complex". Then, these two species react; of the many kinds of processes that could take place, only electron and energy transfer will be considered in the course of this discussion. After the reaction, the products diffuse away from each other. If the two reactants cannot escape the solvent

Daniela M. Arias-Rotondo

Daniela M. Arias-Rotondo was born in Buenos Aires (Argentina). She received her BS in chemistry in 2010 at the University of Buenos Aires, where she conducted research under the guidance of Prof. Luis M. Baraldo. Daniela began her graduate studies in 2010 at Michigan State University, working in the McCusker group. Her research interests include the synthesis and photophysics of coordination compounds, with emphasis on inter- and intramolecular electron and energy transfer.

James K. McCusker

James K. McCusker was born in New Haven, Connecticut in 1965. A graduate of Bucknell University, McCusker obtained his PhD with David N. Hendrickson in 1992 at the University of Illinois at Urbana-Champaign. Following an NIH Post-doctoral Fellowship with Thomas J. Meyer at the University of North Carolina at Chapel Hill, McCusker began his independent career as an Assistant Professor at the University of California at Berkeley. His group was the first to identify the ultrafast processes associated with excited-state formation in Ru(II) polypyridyl complexes. McCusker moved to Michigan State University in 2001 where he is currently Professor of Chemistry. His research continues to focus on the ultrafast excited-state dynamics of transition metal-based chromophores as well as the effects of spin and spin polarization on electron and energy transfer processes.

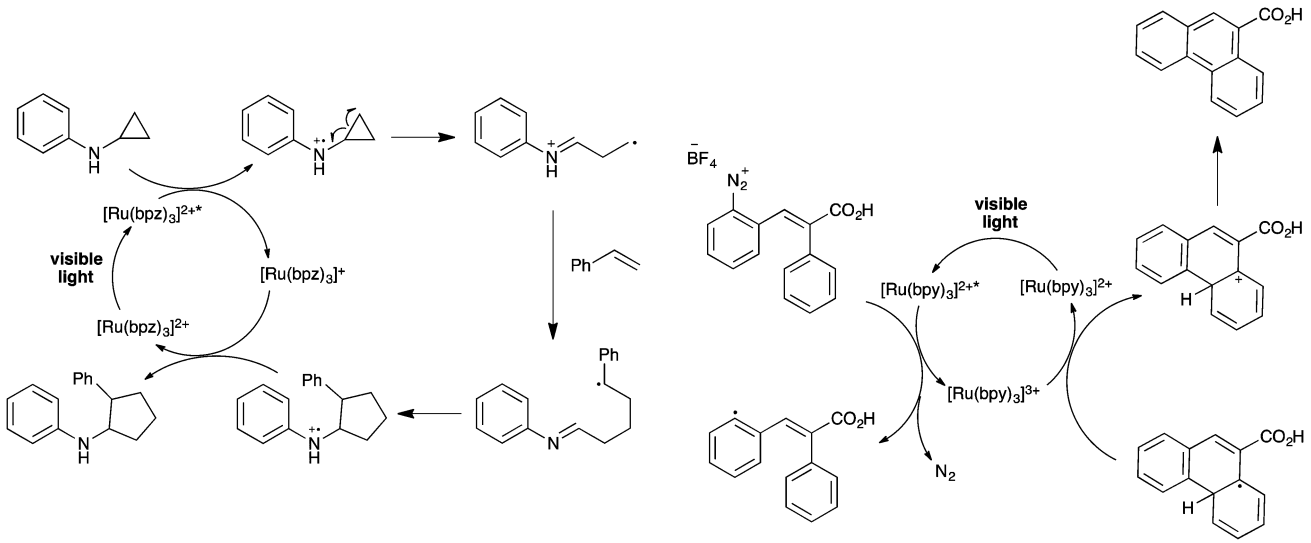

Scheme 1 Examples of a reductive (left) and an oxidative (right) catalytic cycle involving a Ru(II) photocatalyst. Adapted from ref. 13 and 14.

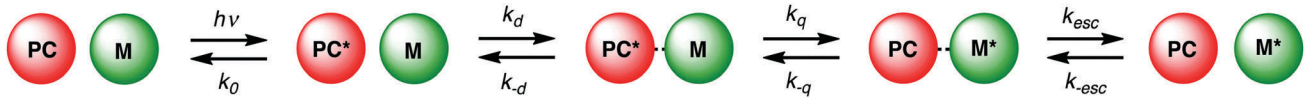

Scheme 2 Simplified kinetic scheme for a general quenching process. Adapted from ref. 2 and 15.

cage fast enough, an unwanted back reaction may take place. This is typically more of a concern with electron (as opposed to energy) transfer processes.

This relatively simple scheme allows us to outline the main points that need to be considered when choosing and/or designing a photocatalyst:

(1) Photocatalytic reactions make use of the enhanced reactivity of the photocatalyst in its excited state. For this reason, a photocatalyst must possess a good absorption cross-section, preferably over a broad range of wavelengths that the other species in the reaction mixture do not absorb.†

(2) The yield of formation of the reactive excited state should be as high as possible. This will be influenced both by the intrinsic quantum yield of its formation (that is, the efficiency with which the reactive excited state is formed upon photon absorption) as well as the absorption cross-section as measured by the compound's concentration and molar absorptivity.

(3) The excited state must persist long enough to undergo the desired reaction with the substrate. In the context of Scheme 2, this means that the excited state of the photocatalyst must have a sufficiently long lifetime to enable it to diffuse to the reactant of interest before relaxing back to the ground state. Diffusion occurs on the nanosecond time scale in most solvents;[16] although increasing the concentration of reagents can offset diffusion to a certain extent, the bimolecular nature of the reaction places a practical upper limit of $\sim 10^9$ s^{-1} for k_0 of the excited photocatalyst.

(4) The photophysics of the photocatalyst must be reversible (*i.e.*, no photodegradation in the absence of quencher). In the case of electron transfer catalysis, the photocatalyst should exhibit reversible electrochemical behavior. Both of these characteristics are needed in order to maintain the viability of the chromophore as part of a catalytic cycle.‡

(5) If the catalytic cycle involves electron transfer, the excited- and ground-state redox potentials of the photocatalyst must provide for an exothermic (or at worst weakly endothermic) reaction.

(6) Ideally, the excited-state properties of the photocatalyst should be easily tuned through synthetic modifications in order to facilitate tailoring the excited-state reactivity of the photocatalyst to the reaction being studied.

Given the various criteria just enumerated, it is no surprise that polypyridyl complexes of Ru(II) and Ir(III) have proven useful as photoredox catalysts. These compounds strongly absorb visible light, which makes it easy to selectively excite them relative to the organic substrates for most reactions of interest. Their excited states are formed with ~100% efficiency[17] and their lifetimes range from 300 ns to 6 μs,[2,3] which is long enough for them to engage in bimolecular reactions. As a class, these compounds are generally stable with respect to decomposition (both photochemical and thermal)§

† Strictly speaking, it is only necessary for the photocatalyst to absorb light of one wavelength that the other species present in the reaction mixture do not absorb; having the photocatalyst absorb over a wider range of wavelengths makes it more versatile.

‡ This is not necessary in the case of an energy-transfer photocatalyst, but those are far less common (see C. K. Prier, D. A. Rankic and D. W. C. MacMillan, *op. cit.* and references therein).

§ Virtually all coordination complexes have a non-zero quantum yield for photodissociation, photosubstitution, *etc.* that eventually leads to decomposition of the chromophore, and Ru(II) and Ir(III) polypyridyl complexes are no exception. However, these compounds are generally more stable than most, particularly in non-coordinating solvents or when isolated as salts with non-coordinating counterions (*e.g.*, PF_6^-).

and typically exhibit reversible redox behavior. They are also emissive, which provides a useful (although not absolutely necessary) handle for mechanistic studies. Finally, there is a vast body of literature describing the synthesis as well as structure/property correlations for this class of compounds, providing an ample database to tap into for the development of chromophores for applications to new chemical transformations.[2,3,18]

As mentioned above, we will build our discussion around the ground- and excited-state properties of $[Ru(bpy)_3]^{2+}$. After detailing the physical and photophysical properties of this compound, we will then focus on the processes that take place during a photocatalytic cycle and provide an overview of the various experimental protocols that allow for discriminating among various mechanistic possibilities. In so doing, our goal is to provide a generalizable blueprint for how to identify, characterize, and ultimately design photocatalysts for use in a wide variety of chemical transformations.

3. $[Ru(bpy)_3]^{2+}$: optical and electrochemical properties

3.1. Optical properties

The electronic absorption spectrum of $[Ru(bpy)_3](PF_6)_2$ in acetonitrile solution is shown in Fig. 1. The intense absorption at 285 nm corresponds to a ligand-centered transition ($\pi_L \rightarrow \pi_L^*$), which has been assigned by comparing it with the absorption spectrum of the protonated ligand.[1] The band in the visible region (λ_{max} = 452 nm) corresponds to a metal-to-ligand charge-transfer (MLCT) transition. As the name implies, this type of excited state can be viewed as the promotion of an electron from a predominantly metal-based orbital to one that is primarily ligand in character. This transition can therefore be thought of as a simultaneous photo-induced oxidation of the metal center and reduction of the ligand that yields a chemical species that can approximately described as $[Ru^{III}(bpy^{\bullet -})(bpy)_2]^{2+*}$ (Scheme 3).[19] Because of this spatial redistribution of electron density, this transition is responsible for the enhanced reactivity of the excited state relative to what is observed in the ground state

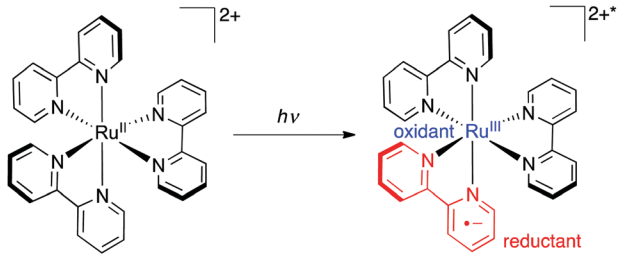

Scheme 3 A qualitative representation of a metal-to-ligand charge-transfer state in $[Ru(bpy)_3]^{2+}$. The spatial separation of charge within the molecule following light absorption is the underlying reason for the redox activity of the excited state.

and makes the compound a viable candidate for a photoredox catalyst. Charge-transfer transitions are typically very intense:[20] for $[Ru(bpy)_3]^{2+}$ in acetonitrile solution at room temperature, the maximum of the MLCT absorption feature corresponds to a molar absorptivity of $\sim$13 000 M^{-1} cm^{-1}.

Two additional features can be seen in the absorption spectrum of $[Ru(bpy)_3]^{2+}$, one at $\sim$330 nm and the other at 350 nm. Their origin(s) have been the subject of considerable debate over the years, but they are most likely due to ligand-field (so-called "d–d") transitions within the d-orbital manifold of the metal. The symmetry-forbidden nature of d–d bands typically limits their absorptivities to the range of 10–100 M^{-1} cm^{-1},[20] but the proximity of both the ligand-centered transitions in the ultraviolet and the MLCT envelope in the visible modulates their intensities in the present case. These metal-centered transitions redistribute electronic density into orbitals that are antibonding with respect to the metal–ligand bonds and therefore typically promote photodissociation.[2] A molecular orbital-based description of these various transitions is shown in Scheme 4.

It is worth noting that most organic substrates, with the exception of highly conjugated systems, do not absorb visible light (*cf.* ligand-based transition in Fig. 1). This allows for selective excitation of the photocatalyst and therefore minimizes the occurrence of unwanted side-reactions.

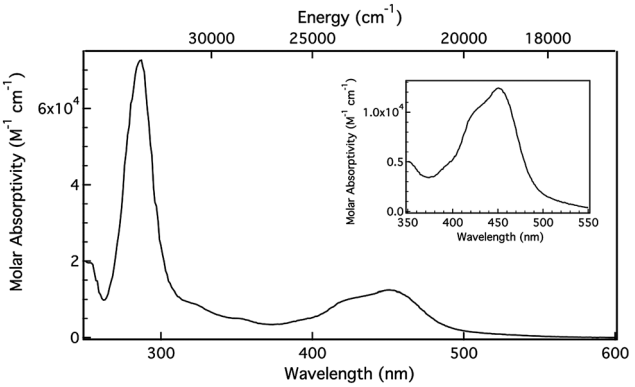

Fig. 1 Electronic absorption spectrum of $[Ru(bpy)_3](PF_6)_2$ in acetonitrile solution at room temperature. The inset shows an expanded view of the metal-to-ligand charge transfer band. See text for details.

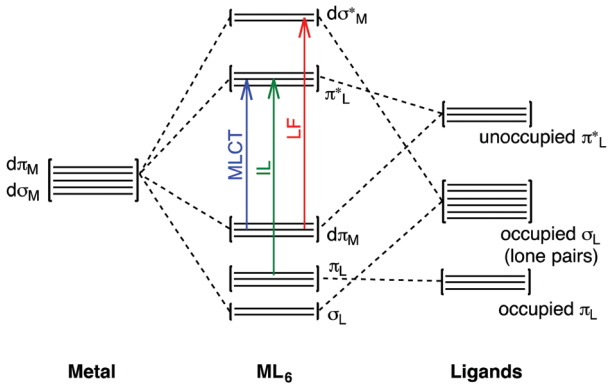

Scheme 4 Simplified molecular orbital diagram for an octahedral compound with π–acceptor ligands. The three main types of electronic transitions typically observed in metal polypyridyl complexes are indicated by the arrows.

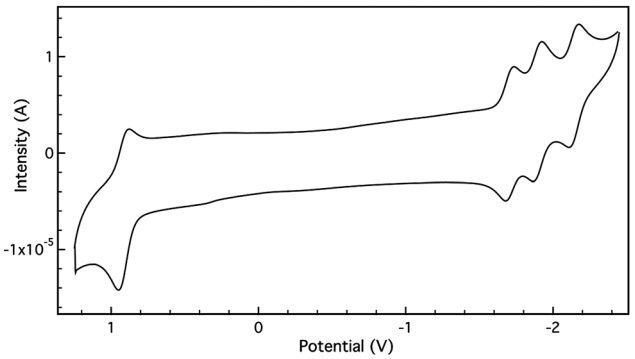

Fig. 2 Cyclic voltammogram of $[Ru(bpy)_3](PF_6)_2$ in CH_3CN, using 0.1 M tetrabutylammonium hexafluorophosphate ($TBAPF_6$) as supporting electrolyte. Potentials are referenced to the ferrocene/ferrocenium couple.

3.2. Electrochemical properties

Photoredox catalysis takes advantage of the ground- and excited-state redox properties of the photocatalyst. Cyclic voltammetry is the most common way to measure the ground-state redox potentials of a compound; the cyclic voltammogram for $[Ru(bpy)_3](PF_6)_2$ in acetonitrile solution is shown in Fig. 2. The oxidation of the metal center (eqn (1)) occurs at $\sim$1 V (referenced to the ferrocene/ferrocenium couple).

$$[Ru(bpy)_3]^{2+} \rightarrow [Ru(bpy)_3]^{3+} + e^- \quad (1)$$

Three reductions are also observed, all of which correspond to one-electron reductions of each of the three ligands in succession (eqn (2a)–(2c)).

$$[Ru(bpy)_3]^{2+} + e^- \rightarrow [Ru(bpy^{\bullet -})(bpy)_2]^{+} \quad (2a)$$

$$[Ru(bpy^{\bullet -})(bpy)_2]^{+} + e^- \rightarrow [Ru(bpy^{\bullet -})_2(bpy)] \quad (2b)$$

$$[Ru(bpy^{\bullet -})_2(bpy)] + e^- \rightarrow [Ru(bpy^{\bullet -})_3]^{-} \quad (2c)$$

The first two reductions as well as the metal-centered oxidation are reversible, where reversibility is defined by the difference in anodic and cathodic peak potentials (ideally 59 mV for a one-electron process, but more typically in the range of 70–80 mV in non-aqueous media),¶ as well as a cathodic/anodic peak current ratio close to unity. By these metrics, the last reduction (eqn (2c)) is quasi-reversible at best. In terms of photoredox reactions, only the first reduction (*i.e.*, eqn (2a)) will be relevant for one-electron processes, but the reversibility of these redox processes is an important consideration when these compounds are used as photocatalysts, since the photocatalyst must be stable enough in its oxidized or reduced form in order to be regenerated over the course of multiple turnovers of a given reaction.

¶ The peak separation for a given redox couple may be affected by variables such as the solvent employed and the geometry of the electrode configuration. The ferrocene/ferrocenium couple is considered completely reversible in non-aqueous media. As such, its peak separation in a given experiment can be used as a criterion for reversibility for other redox processes as long as the experimental conditions are the same for all the measurements.

Using the description above, the energy of the ^{1}MLCT band can be thought of as the amount of energy necessary to reduce the ligand and oxidize the metal:

$$E(\text{MLCT}) = |E(Ru^{III}/Ru^{II})| + |E(bpy/bpy^{\bullet -})| \quad (3)$$

Several aspects of eqn (3) are worth noting: (1) this is an approximation: energetics associated with solvation as well as electron correlation effects are not accounted for in this simplified expression;[21] (2) the fact that there are two contributions to the MLCT energy – the oxidation potential of the metal and the reduction potential of the ligand – implies that the value of E(MLCT) alone is not sufficient to determine whether a chromphore's energetics are suitable for a given reaction. One can observe MLCT bands at roughly the same energy where one arises from a very strong reductant (*i.e.*, very negative ligand reduction potential) coupled with a very weak oxidant, or *vice versa*. The electrochemical data on the compound is one of the ways by which these important details can be deconvolved.

4. Excited-state kinetics

We are ultimately interested in bimolecular reactions between an excited photocatalyst and an organic molecule. Before we can discuss these processes, however, it is necessary to understand the excited-state properties of the photocatalyst in the absence of a substrate, since the presence (or absence) of a reaction will ultimately be determined by referring back to the photocatalysts' intrinsic excited-state behavior.

In a one-electron approximation (*e.g.*, Scheme 4), the electronic configuration of the excited state is obtained by simply taking an electron from an occupied orbital in the ground state and placing it in an empty orbital of higher energy. Although this is useful as a first approximation – particularly with regard to developing chemical intuition concerning the potential reactivity of the excited state – this picture has a number of significant deficiencies. First, the geometry of the molecule in the excited state will be different from that of the ground state. Second, electronic correlation effects (*e.g.*, electron–electron repulsion) significantly modulate both ground- and excited-state energetics in ways distinct from what is inferred from orbital energies. In other words, there is not a one-to-one correlation between differences in orbital energies and the energy of a given electronic excited state. Finally, this approximation does not account for spin, which is important for understanding electronic absorption spectra[20] as well as accounting for conservation of angular momentum for a given reaction. So, while a molecular orbital diagram such as the one shown in Scheme 4 is a useful construct in terms of understanding the chemical nature of an electronic excited state, electronic transitions and the photophysics/photochemistry of excited states are best viewed in terms of potential energy surface diagrams. One such diagram is shown in Scheme 5, where parabolic curves are used to represent the various electronic states that arise from Scheme 4 coupled with consideration of electron–electron interactions and any changes

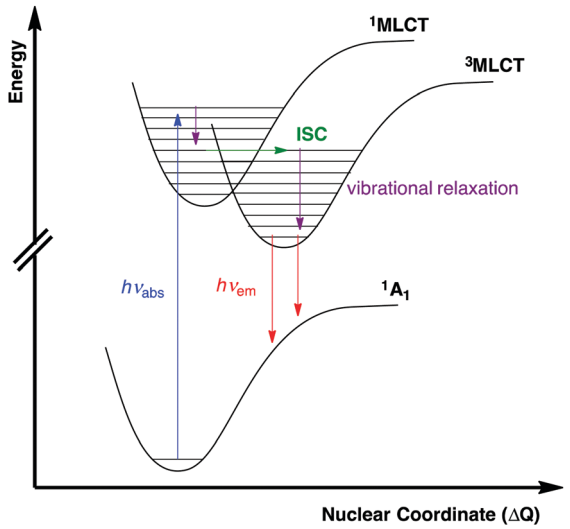

Scheme 5 Simplified potential energy surface diagram for $[Ru(bpy)_3]^{2+}$. See text for details.

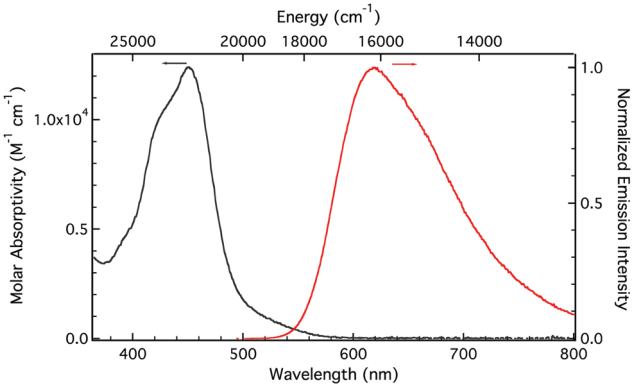

Fig. 3 Electronic absorption spectrum (gray) and steady state emission spectrum (red) of $[Ru(bpy)_3](PF_6)_2$ in acetonitrile solution at room temperature.

in equilibrium geometry. The diagram shown in Scheme 5 only includes MLCT transitions and is appropriate for compounds like $[Ru(bpy)_3]^{2+}$ where the MLCT excited states are the ones relevant for photoredox catalysis.

4.1. Steady-state emission

As shown in Scheme 5, visible light excites $[Ru(bpy)_3]^{2+}$ into a ^{1}MLCT state; this short-lived state relaxes to a ^{3}MLCT state within ~100 fs *via* intersystem crossing (ISC, with rate constant k_{isc}).[22] The ^{3}MLCT state can relax back to the ground state either non-radiatively (with rate constant k_{nr}) or *via* phosphorescence (a radiative pathway with rate constant k_r). Eqn (4) through (6) illustrate these processes.

$$\left[Ru^{II}(bpy)_3\right]^{2+} \xrightarrow{h\nu_{abs}} {}^1\left[Ru^{III}(bpy^{\bullet-})(bpy)_2\right]^{2+*} \quad (4a)$$

$${}^1\left[Ru^{III}(bpy^{\bullet-})(bpy)_2\right]^{2+*} \xrightarrow{k_{isc}} {}^3\left[Ru^{III}(bpy^{\bullet-})(bpy)_2\right]^{2+*} \quad (4b)$$

$$\left[Ru^{III}(bpy^{\bullet-})(bpy)_2\right]^{2+*} \xrightarrow{k_r} \left[Ru^{II}(bpy)_3\right]^{2+} + h\nu_{em} \quad (5)$$

$$\left[Ru^{III}(bpy^{\bullet-})(bpy)_2\right]^{2+*} \xrightarrow{k_{nr}} \left[Ru^{II}(bpy)_3\right]^{2+} + \text{heat} \quad (6)$$

Photoinduced reactions, such as the coordination of a solvent molecule or the loss of a ligand, can also take place. However, these are not usually observed for $[Ru(bpy)_3]^{2+}$ and related compounds,[17] so they will not be discussed here.

The solution-phase steady-state emission spectrum of $[Ru(bpy)_3]^{2+}$ at room temperature is shown in Fig. 3: the emission maximum is at 620 nm. The same spectrum is obtained regardless of the excitation wavelength, consistent with the near-unit quantum yield of formation of the emissive ^{3}MLCT state.[17]

The emission maximum can be used as a first-order approximation of E_0, the energy difference between the triplet excited state (^{3}MLCT) and the ground state. This value (E_0) is usually associated with the highest energy vibrational component of the emission spectrum at 77 K (which may or may not correspond to the observed emission maximum).[21] Regardless, E_0 can be accurately determined by a single mode fit of the steady-state emission spectrum using eqn (7), as described by Claude and Meyer.[23,24]

$$I(\bar{\nu}) = \sum_{\nu_M=0}^{5}\left\{\left(\frac{E_0 - \nu_M\hbar\omega_M}{E_0}\right)^3 \frac{S_M^{\nu_M}}{\nu_M!} \times \exp\left(-4(\ln 2)\left(\frac{\bar{\nu} - E_0 + \nu_M\hbar\omega_M}{\Delta\bar{\nu}_{0,1/2}}\right)^2\right)\right\} \quad (7)$$

A discussion of the various parameters in this expression is beyond the scope of this Tutorial but can be found in the work of Claude and Meyer.[23,24] The value of E_0 is an important quantity: in addition to quantifying the added free energy that light absorption affords, the zero-point energy of the excited state is needed in order to assess the thermodynamic viability of a given photoredox reaction. This will be discussed in greater detail in the Designing photocatalysts section.

For an emissive substance, the simplest definition of the quantum yield (Φ) of emission (also called the radiative quantum yield) is the ratio between the number of photons emitted by a sample and the number of photons absorbed, as shown in eqn (8).

$$\Phi = \frac{\#\text{ photons emitted}}{\#\text{ photons absorbed}} = \frac{I_{em}}{I_{abs}} \quad (8)$$

The radiative quantum yield can also be described in terms of a kinetic competition, specifically the relative rate(s) of processes giving rise to emission *versus* the rates of all processes that serve to deplete the population of that emissive state. Referring to eqn (5) and (6), in the absence of any species other than the chromophore, Φ can be expressed as:

$$\Phi_0 = \frac{k_r}{k_r + k_{nr}} = \frac{k_r}{k_0} \quad (9)$$

where $k_0 = k_{nr} + k_r$.

Radiative quantum yields can be measured as absolute values (*i.e.*, eqn (8)) or relative to some standard. To measure an absolute quantum yield it is necessary to detect every photon that is emitted by the sample, which tends to be quite labor intensive. Although instrumentation has recently become commercially available to allow for (relatively) facile measurement of absolute radiative quantum yields,‖ most of the quantum yields in literature are determined and reported relative to a standard with a known absolute value.[25] $[Ru(bpy)_3]^{2+}$ is commonly used as a standard for relative quantum yields of transition metal complexes; its quantum yield in deoxygenated** acetonitrile at room temperature is 0.095.[26]

The relative quantum yield of a sample can be calculated using eqn (10),

$$\Phi_x = \Phi_{std}\left(\frac{I_x/A_x}{I_{std}/A_{std}}\right)\left(\frac{\eta_x}{\eta_{std}}\right)^2 \quad (10)$$

where x refers to the molecule of interest and std to the standard; I_x and I_{std} are the integrated areas of the corrected†† emission spectra, A_x and A_{std} are the absorbances at the excitation wavelength, and η_x and η_{std} are the indices of refraction of the solutions (usually assumed to be equal to those of the neat solvents). The choice of a standard depends on the emission properties of the molecule of interest; it is best if the standard and the molecule are dissolved in the same solvent and have similar absorption and emission spectra. For relative quantum yield determinations, it is crucial that the experimental conditions for both the sample and the standard are exactly the same. A more detailed discussion of methodology for measuring and quantifying emission data is beyond the scope of this review, but a number of excellent resources are readily available.[25,27]

4.2. Kinetics: time-resolved emission

Both the radiative and non-radiative decay processes (eqn (5) and (6)) are first-order with respect to the excited state (ES) and give rise to the following expression for the rate at which that excited state is lost,

$$-\frac{d[ES]}{dt} = k_r[ES] + k_{nr}[ES] = (k_r + k_{nr})[ES] = k_0[ES] \quad (11)$$

this equation can be integrated to yield the rate law for a first-order reaction, shown in eqn (12).

$$[ES] = [ES]_0 e^{-k_0 t} \quad (12)$$

The inverse of the observed rate constant, k_0^{-1}, is the lifetime (τ_0) of the excited state; for an emissive complex, this can be easily measured using time-resolved emission spectroscopy. (For non-emissive compounds, excited-state lifetimes can be determined using time-resolved absorption methods. This will be discussed in greater detail in the Probing the mechanism, stage II section).

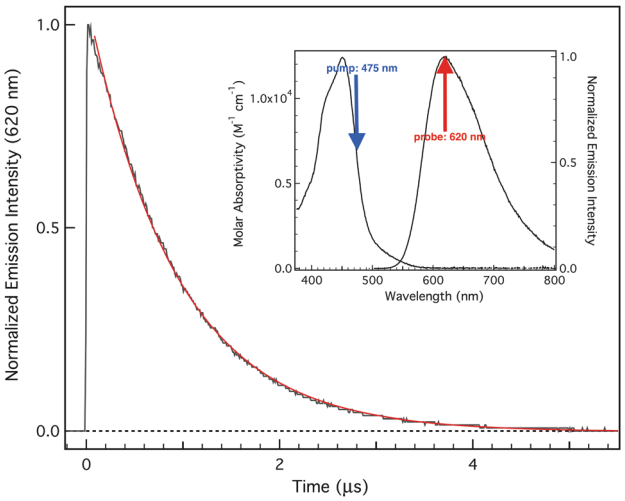

Fig. 4 Time-resolved emission data (grey line) for $[Ru(bpy)_3]^{2+}$ in acetonitrile solution at room temperature. The sample was excited at 475 nm and emission was detected at 620 nm (as shown in the inset). The red trace shows the fit to a single exponential decay with τ = 930 ns.

In a time-resolved emission experiment, the sample is excited at a wavelength at or near its absorption maximum, with the emission collected at 90° with respect to the excitation beam in order to minimize scatter. A typical time-resolved emission trace for $[Ru(bpy)_3]^{2+}$ in acetonitrile is shown in Fig. 4; τ_0 can be found by fitting the trace to a single exponential decay. For $[Ru(bpy)_3]^{2+}$, the lifetime ranges between 500–1000 ns, depending on a number of variables including solvent, oxygen concentration in the sample, temperature, *etc.*[2] In deoxygenated acetonitrile at room temperature, the lifetime of $[Ru(bpy)_3]^{2+}$ is 930 ± 40 ns.‡‡

Combining the excited-state lifetime and the radiative quantum yield, it is possible to calculate k_r and k_{nr}. Rearranging eqn (9), we obtain (13) and (14).

$$k_r = \Phi_0 \times k_0 \quad (13)$$

$$k_{nr} = k_0 - (\Phi_0 \times k_0) = k_0 \times (1 - \Phi_0) \quad (14)$$

It is important to highlight that k_r is an intrinsic property of the molecule and therefore remains constant no matter what reactions the excited state engages in. On the other hand, k_{nr} varies when quenching processes (such as energy or electron transfer) take place. All of the information that we will be interested in for a photocatalytic cycle (in other words, the information about any processes competing with the emission) is contained in k_{nr}; in this regard, k_r can be viewed as a probe, providing insight into the dynamics of the system being

‖ Recently, Hamamatsu (http://www.hamamatsu.com) has developed instruments that can measure absolute quantum yields easily in minutes. However, these instruments' level of detection is such that quantum yields lower than 5% are almost undetectable.

** This is necessary because O_2 can quench the ^{3}MLCT excited state of $[Ru(bpy)_3]^{2+}$.

†† Spectra refer to emission spectra that have been properly corrected for the fluorimeter's instrument response characteristics. References on emission spectroscopy can be consulted for further information on this point.

‡‡ The error bars for this value are obtained from the fits of several datasets.

manifested in k_{nr}. This concept is discussed in greater detail in the Quenching studies section.

5. Excited-state reactivity of $[Ru(bpy)_3]^{2+}$

In its excited state, $[Ru(bpy)_3]^{2+}$ can act as an energy donor, an electron acceptor or an electron donor; thermodynamic and kinetic factors associated with a given reaction determine which process dominates.[28]

The inherent competition that exists among these various reaction pathways is depicted in eqn (15a)–(15c); the energy transfer route can furthermore be subdivided according to the specific mechanism by which it proceeds. As a result, although determining that the excited state of the chromophore is reacting can be as straightforward as observing emission quenching, mechanistic discrimination as to the nature of that reaction generally requires considerably more work, as will be described in the next few sections.

$$[Ru^{III}(bpy^{\bullet-})(bpy)_2]^{2+*} \xrightarrow[k_{EnT}]{+\,Q} [Ru^{II}(bpy)_3]^{2+} + Q^* \quad (15a)$$

$$[Ru^{III}(bpy^{\bullet-})(bpy)_2]^{2+*} \xrightarrow[k_{ox}]{+\,A} [Ru^{III}(bpy)_3]^{3+} + A^{\bullet-} \quad (15b)$$

$$[Ru^{III}(bpy^{\bullet-})(bpy)_2]^{2+*} \xrightarrow[k_{red}]{+\,D} [Ru^{II}(bpy^{\bullet-})(bpy)_2]^{+} + D^{\bullet+} \quad (15c)$$

5.1. Energy transfer: Förster and Dexter mechanisms

Energy transfer is a process by which excess energy contained in one molecule (the donor) is transferred to another molecule (the acceptor). In the context of the chemical systems being discussed herein, that excess energy comes from the absorption of a photon by the donor to create an electronic excited state. The product of the reaction is an electronically excited acceptor molecule concomitant with reformation of the electronic ground state of the donor, as shown in eqn (16).

$$D^* + A \xrightarrow{k_{EnT}} D + A^* \quad (16)$$

Although energy transfer can occur as the result of emission from the donor and subsequent absorption of that emitted light by the acceptor (the so-called "trivial" mechanism), energy transfer more typically occurs *via* non-radiative processes (that is, the emission and reabsorption of light do not occur). The two most common mechanisms of non-radiative energy transfer are known as Förster (through-space) and Dexter (through-bond or "exchange") energy transfer. These mechanisms are depicted in Scheme 6. It should be noted that both Förster and Dexter transfer yield the same products (*i.e.* ground-state donor and excited-state acceptor), although the physical origins of the reaction are fundamentally different.[16]

Förster energy transfer[29] is a dipolar mechanism that takes place through space: the transition moment dipole of the donor couples non-radiatively with the transition moment dipole of the acceptor (see Scheme 7). Because of the dipolar nature of this mechanism, no orbital overlap is necessary between the donor and the acceptor. This makes Förster energy transfer operational over distances that can range from 10 to 100 Å.[30]

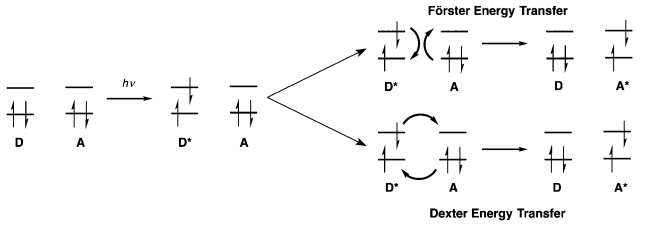

Scheme 6 Förster and Dexter energy transfer mechanisms.

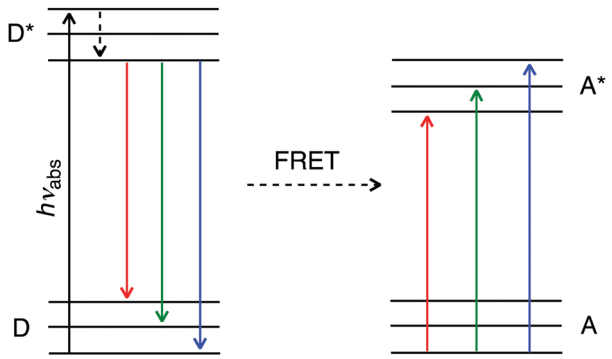

Scheme 7 Simplified diagram showing the coupling of the donor (D) and acceptor (A) transition dipoles. Transitions represented in the same color are coupled together.

An overlap between the emission spectrum of the donor and the electronic absorption spectrum of the acceptor is necessary for the energy transfer to occur; this resonance condition (which in reality is simply a reflection of energy conservation for this process) is represented in Scheme 8. Because of this condition, Förster transfer is often referred to as Fluorescence Resonance Energy Transfer (FRET). As was previously mentioned, the organic substrates usually involved in photocatalyzed reactions do not typically absorb light in the visible region of the spectrum, so the spectral overlap between their absorption spectrum and the emission spectrum of $[Ru(bpy)_3]^{2+}$ is negligible. As a consequence, Förster energy transfer is not a common reaction pathway for the systems being considered herein.

The rate constant for Förster energy transfer can be expressed as shown in eqn (17),[31]

$$k_{FRET} = k_0^D \left(\frac{9000(\ln 10)\kappa^2 \Phi_D I}{128\pi^5 N \eta^4}\right)\frac{1}{R^6} \quad (17)$$

where k_0^D and Φ_D are the observed rate constant of the donor and its corresponding emission quantum yield (both in the absence of the acceptor), N is Avogadro's number, η is the refractive index of the medium, I is the spectral overlap integral,[31] and R is the distance between the donor and the acceptor. The factor κ is related to the relative orientation of the dipoles associated with the donor's emission and the acceptor's absorption transitions. This orientation parameter can take on any value between 0 and 4; for a bimolecular reaction between two freely rotating molecules in solution,

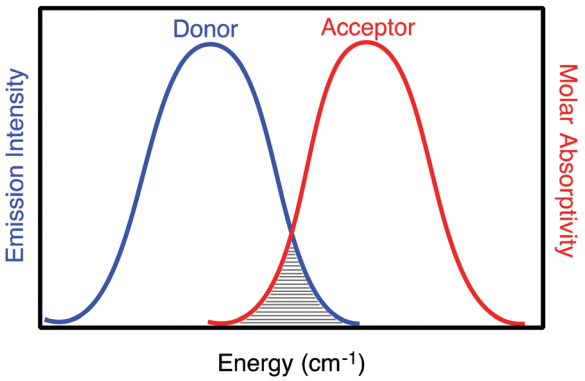

Scheme 8 Schematic emission spectrum of the donor and absorption spectrum of the acceptor. The shaded region is the spectral overlap reflecting the resonance condition needed for Förster energy transfer to occur.

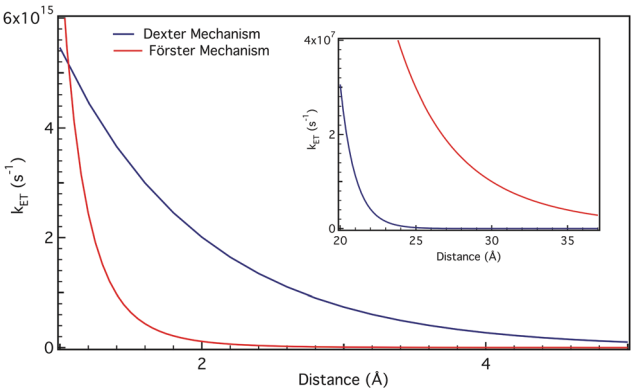

Fig. 5 Simulated plot of the rate constant as a function of the donor–acceptor distance for Dexter (blue) and Förster (red) mechanisms. The inset shows the prevalence of FRET at longer distances. For Förster energy transfer $k_r^D = 10^7\ s^{-1}$ and $R_0 = 30$ Å (arbitrarily chosen); for Dexter energy transfer, $A = 1$, $\beta = 1$ Å^{-1} and $r_c = 5$ Å.[27]

a value of 2/3 is appropriate. A more detailed discussion of the application of the Förster equation in donor–acceptor systems can be found elsewhere.[31]

Using the definition of radiative quantum yield (eqn (9)), eqn (17) can be written as:

$$k_{FRET} = k_r^D \left(\frac{R_0}{R}\right)^6 \quad (18)$$

where R_0 is the critical transfer distance (often called the Förster radius):[16]

$$R_0 = \frac{9000(\ln 10)\kappa^2 I}{128\pi^5 N\eta^4} = \frac{8.79\times10^{-25}\kappa^2 I}{\eta^4} \quad (19)$$

The Dexter mechanism,[32,33] on the other hand, is best thought of as two simultaneous electron transfer reactions (Scheme 6). Except in rare cases, electron transfer is a through-bond process, meaning that Dexter energy transfer requires orbital overlap between the donor and the acceptor in order to occur: this limits its prevalence to reactions taking place at much shorter distances than the Förster mechanism (typically no more than 10 Å). In other words, for a bimolecular reaction the Dexter process requires physical contact between the excited donor and the acceptor. On the plus side, since it is an exchange process (as opposed to a resonance one), the spectral resonance condition depicted in Scheme 8 is lifted: only the relative energies of the electronic states involved in the reaction is relevant for defining a thermodynamically viable reaction.

Molecular oxygen can quench the excited state of many transition-metal polypyridyl compounds *via* Dexter energy transfer.[34,35] For this reason, most photophysical measurements involving $[Ru(bpy)_3]^{2+}$ and other transition-metal complexes are carried out in deoxygenated solutions.

Due to the fact that Dexter energy transfer is dependent upon orbital overlap, its distance dependence is exponential,

$$k_{DET} = A\exp(-\beta(r - r_c)) \quad (20)$$

where r_c is the distance of closest approach at molecular contact[27] and β is an attenuation factor (typically $\beta \leq 1$ Å^{-1}).[36]

The impact of the dramatic difference in the nature of the distance dependence for these two mechanisms is illustrated in Fig. 5, in which we have simulated the rate of energy transfer (k_{ET}) as a function of donor–acceptor distance. As the plot shows, the Dexter mechanism is only significant (even dominant) at very short distances, whereas the Förster mechanism can be operative over much longer distances.

5.2. Electron transfer

A generic electron transfer process can be represented as:

$$D + A \xrightarrow{k_{ET}} D^+ + A^- \quad (21)$$

Although electron transfer can be accompanied by bond breaking and/or formation, in photoredox catalysis we are usually interested in reactions where the structure and composition of both the donor and acceptor remain largely intact.

The kinetics of electron transfer can be described using Marcus theory,[37] where the rate constant for outer sphere electron transfer can be written as shown in eqn (22).

$$k_{ET} = \frac{2\pi}{\hbar}|H_{AB}|^2 \frac{1}{\sqrt{4\pi\lambda k_B T}} \exp\left[\frac{(-\Delta G^\circ + \lambda)^2}{4\lambda k_B T}\right] \quad (22)$$

In this expression, ΔG° is the driving force for electron transfer (which depends on the redox potentials of the donor and the acceptor), H_{AB} represents the electronic coupling between the donor and the acceptor, and λ is the reorganization energy. This latter term reflects energetics associated with the structural changes linked to oxidizing the donor and reducing the acceptor, as well as the reorganization of the solvent molecules due to the redistribution of charge that accompanies electron transfer. The magnitude of the electronic coupling (H_{AB}) depends on the distance and orientation of donor and acceptor and therefore tends to be difficult to specify for bimolecular reactions in solution.

Even though electron transfer and Dexter energy transfer are closely related, two important differences should be noted. First, because two electrons are exchanged instead of one, Dexter energy transfer has a much steeper distance dependence than electron transfer (typically e^{-2r} as opposed to e^{-r} for electron transfer).[33] Second, since electron transfer leads to a new charge distribution, its reorganization energy (especially the solvent contribution) is much larger than that associated with Dexter (or for that matter Förster) energy transfer.[38]

Notwithstanding these details, the important point to appreciate is that the products formed following energy *versus* electron transfer are chemically distinct. This difference will provide a means for experimentally differentiating these two reaction pathways.

6. Probing the mechanism, stage I: Stern–Volmer quenching studies

When investigating possible reaction mechanisms, the simplest experiment that can be performed is a Stern–Volmer quenching study. This experiment allows one to determine whether a reaction is occurring between the excited state of the photocatalyst and one (or more) of the substrates. While this is extremely useful information, it is important to stress that very little mechanistic information is afforded by a Stern–Volmer study, with the possible exception of identifying static *versus* dynamic contributions to the quenching (*vide infra*). As will become apparent in the discussion to follow, *both energy and electron transfer reactions involving the excited state of the chromophore will yield experimentally indistinguishable results from a Stern–Volmer quenching study*. It is only through the application of additional experiments (most notably time-resolved absorption spectroscopy) that further insight into the nature of the reaction responsible for the quenching can be gleaned.

In the context of an emissive species, the term "quenching" refers to any process that reduces the radiative quantum yield of a fluorophore. Not surprisingly, there is a wide variety of processes that could fall into this category, but only a few of which are relevant to our discussion. Dynamic (or collisional) quenching consists in a bimolecular reaction between the excited chromophore and the quencher, whereas static quenching refers to process(es) that do not require diffusion of the reactants involved (*e.g.*, a pre-association between the chromophore and the quencher prior to light absorption). Dynamic quenching can be quantified using time-resolved spectroscopic methods whereas static quenching is most clearly manifest using steady-state techniques (*e.g.*, emission quantum yields). Ultimately, both methods should be employed in order to obtain a complete accounting of all of the contributions to quenching in a given system.

In the Excited-state kinetics section, the radiative and non-radiative pathways for the excited state were described. When a molecule other than the photoactive species is present in solution, the possibility of additional reactions (*e.g.*, electron and/or energy transfer) is introduced. In a very general way, we can represent this situation in the following way:

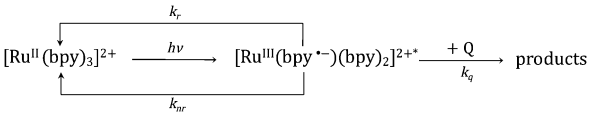

(23)

where Q represents the quencher/substrate. In this scheme, the rate at which the excited state disappears is given by eqn (24).

$$-\frac{d[ES]}{dt} = k_0[ES] + k_q[ES][Q] \quad (24)$$

"Quenching", then, refers to a situation in which $k_q[Q]$ is sufficiently large relative to k_0 such that the observed lifetime of the excited state is measurably attenuated relative to its value in the absence of quencher. This condition is usually met provided the excited state lifetime is on the nanosecond time scale (or longer). Photocatalysts with sub-nanosecond lifetimes are more problematic because of the likelihood that the excited state will relax back to the ground state before it can diffuse to and react with the substrate.[19] Quantifying k_q is most easily done by carrying out measurements under pseudo first-order conditions: if the concentration of the quencher is at least one to two orders of magnitude larger than that of the photocatalyst,§§ [Q] can be assumed to be constant throughout the experiment. Under these conditions, eqn (24) collapses to eqn (25) and allows for the determination of k_q (eqn (26)).

$$-\frac{d[ES]}{dt} = (k_0 + k_q[Q])[ES] = k_{obs}[ES] \quad (25)$$

$$k_{obs} = (k_0 + k_q[Q]) \quad (26)$$

Based on eqn (26), k_{obs} is now a concentration-dependent quantity reflecting both the intrinsic lifetime of the excited state and the extent to which the presence of the quencher introduces a kinetically competitive relaxation pathway. If the sensitizer is emissive, k_{obs} is most easily measured *via* time-resolved emission spectroscopy: by measuring the decay rate constant at several quencher concentrations, the quenching constant k_q can be determined by plotting k_{obs} as a function of quencher concentration as shown in the Stern–Volmer equation (eqn (27)).

$$\frac{k_{obs}}{k_0} = \frac{k_0 + k_q[Q]}{k_0} = 1 + \frac{k_q[Q]}{k_0} \quad (27)$$

Thus, a plot of k_{obs}/k_0 *versus* [Q] should always yield a straight line with an intercept of 1 and a slope equal to k_q/k_0. Any significant deviations from linearity and/or an intercept value of 1 should be viewed as an indication of a problem with the data, the data workup, or, potentially, of a more complex reaction than represented by eqn (25).

Alternatively, steady-state emission spectroscopy may be employed; in this case, the radiative quantum yield of the

§§ Strictly, it must be [Q] ≫ [ES], but since evaluating the concentration of the excited state is not trivial, it is simpler to make [Q] ≫ [photocatalyst].

photocatalyst in the presence of a quencher depends on k_q and [Q] as shown in eqn (28).

$$\Phi_q = \frac{k_r}{k_0 + k_q[Q]} \quad (28)$$

Provided that the radiative quantum yields for the chromophore in the presence and absence of the quencher are determined under identical experimental conditions, their ratio can be related to the Stern–Volmer expression (eqn (29)).

$$\frac{\Phi_0}{\Phi_q} = \frac{k_0 + k_q[Q]}{k_0} = 1 + \frac{k_q[Q]}{k_0} \quad (29)$$

Assuming that the rate constant for excited-state decay of the chromophore (k_0) is known, k_q can be determined by measuring the radiative quantum yield as a function of quencher concentration. It is important to underscore that for the results of this experiment to be meaningful, quantum yields (calculated using eqn (10)) must be used in eqn (29). Alternatively, this can be simplified by using the emission intensity normalized by the absorbance of the chromophore in the sample (*i.e.*, I_x/A_x in eqn (10)). A common mistake is to use emission intensities that have not been properly normalized. There are two scenarios where this can become an issue. The first arises if the quencher and the photocatalyst both absorb at the excitation wavelength. In this case, the total absorbance of the sample is partitioned between the chromophore and the quencher (*i.e.*, the absorbance is additive as long as the photocatalyst and the quencher do not interact significantly).[27] Less light being absorbed by the photocatalyst means less intense emission, which can give the impression of quenching even if no reaction is taking place. In most cases there is very little overlap between a photocatalyst absorbing in the visible and an organic substrate, but as the relative concentration of substrate is increased over the course of a Stern–Volmer measurement, what was a small amount of overlap under equal concentration conditions can be come significant. For this reason, it is important to know the molar absorptivities and concentrations of all of the components absorbing at the excitation wavelength so appropriate corrections can be made. The second scenario is more common and can arise even if the absorption of the photocatalyst is well isolated. When making samples for Stern–Volmer studies, the concentration of the quencher is typically increased at the expense of the concentration of chromophore. The more dilute the chromophore is in the sample, the lower its emission intensity will be, regardless of any quenching that might occur. As with first scenario just described, this situation will make it appear as if the emission of the photocatalyst is even more quenched than it actually is. Dividing the emission intensity by the absorbance of chromophore in the sample eliminates this dilution effect.

As was mentioned above, two kinds of quenching (static and dynamic) are possible. Fig. 6 shows simulated Stern–Volmer plots using time-resolved and steady-state emission data for three different scenarios: (1) dynamic quenching (Fig. 6a); (2) static quenching (Fig. 6b); and (3) both dynamic and static quenching simultaneously present (Fig. 6c). If only dynamic quenching takes place between the chromophore and the substrate, the Stern–Volmer plots derived from steady-state and time-resolved emission measurements will be indistinguishable from one another, as seen in Fig. 6a. In other words, in this scenario eqn (27) and (29) are equivalent and the ratio k_q/k_0 is typically denoted as K_D, the dynamic quenching constant.

Static quenching occurs when the chromophore and the quencher are associated in the ground state. This will typically not have an effect on the lifetime of the chromophore (that is, $k_{obs} = k_0$): the Stern–Volmer plot derived from time-resolved emission will therefore be a flat line (Fig. 6b). This type of quenching will manifest in the time-resolved data as a decrease in the initial amplitude of the signal (*i.e.*, A_0 in the single-exponential fit to determine k_{obs}), but quantifying the signal amplitude in this way from a kinetic trace tends to be unreliable. Instead, measurements of the radiative quantum yield as a function of quencher concentration will yield a linear Stern–Volmer plot consistent with eqn (29). In this case, k_q/k_0 is usually designated as K_S, the static quenching constant.

Finally, if static and dynamic contributions to the quenching are present, both the quantum yield and the lifetime of the excited state will be affected, albeit not in the same way. As shown in Fig. 6c, the Stern–Volmer plot based on time-resolved emission data will yield a straight line, being only influenced by the dynamic contributions to the quenching. The plot based on radiative quantum yield data, on the other hand, will reflect contributions from both static and dynamic processes and will display a quadratic relationship between Φ_0/Φ_q and [Q], as shown in Fig. 6c and eqn (30),

$$\frac{\Phi_0}{\Phi_q} = (1 + K_D[Q])(1 + K_S[Q]) \quad (30)$$

where K_D and K_S are as previously defined.

The availability of both steady-state and time-resolved quenching data, however, allows for a complete analysis of the kinetics.

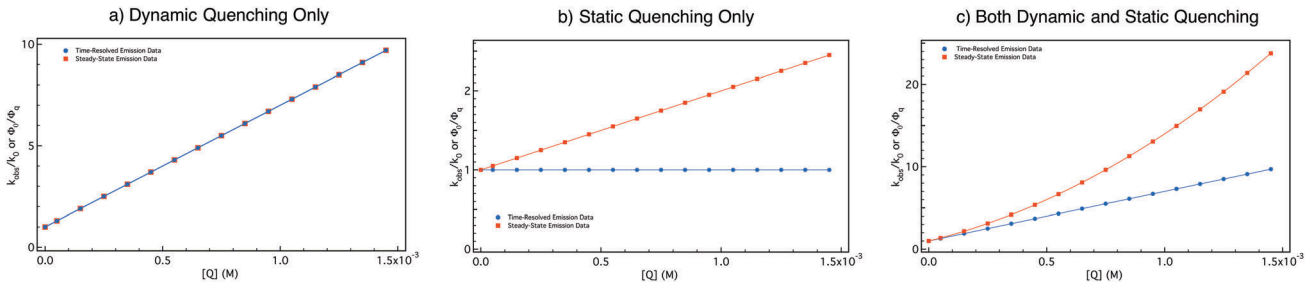

Fig. 6 Simulated Stern–Volmer plots based on time-resolved (blue) and steady-state (red) emission experiments. The lines correspond to the fits according to eqn (27), (29) or (30). For these simulations, K_D = 6000 M^{-1} and K_S = 1000 M^{-1}. See text for details.

As mentioned previously, K_D is the slope of the Stern–Volmer plot based on time-resolved experiments (eqn (27)), which allows K_S to be calculated using the quadratic fit of the steady-state Stern–Volmer plot and the value for K_D obtained from the linear fit of the time-resolved data.

It is important to notice that nowhere in the above discussion was the nature of the quenching mechanism considered. Stern–Volmer studies are helpful because the excited state lifetime is shortened if a reaction between the excited photocatalyst and a quencher is taking place. However, the only information these studies can provide is whether or not the excited state is engaging in a reaction. *They do not in any way provide mechanistic insights because energy and electron transfer quenching pathways will yield qualitatively indistinguishable results for this experiment.*¶¶

7. Probing the mechanism, stage II: identifying the nature of the excited state reaction

The preceding discussion emphasized that a Stern–Volmer study does not provide any insight into the actual reaction the excited state of a sensitizer is engaging in. A simple analogy can be drawn with, for example, the hydrogenation of an alkene. If one used ^{1}H NMR to probe this reaction, the disappearance of the vinyl proton(s) resonance(s) would never be used as proof that the alkane had formed, only that a reaction involving the olefin had taken place. In the same way, the observation of quenching of emission from the sensitizer in a Stern–Volmer quenching study is nothing more than evidence that the starting material (*i.e.*, the excited state) is being consumed. In order to determine what reaction actually occurred, one must identify the product(s) of the reaction.

In the context of photoredox catalysis, dynamic quenching is far more important for the reaction to proceed than static quenching. Therefore, in this and the following sections we will assume that only dynamic quenching is taking place.

As mentioned previously, the two dominant reaction pathways available in most systems are electron and energy transfer between the excited photocatalyst and the substrate/quencher; in the case of the former, oxidative and reductive quenching are both possible, with each leading to distinctly different products. In the case of energy transfer, the photocatalyst will go back to the ground state (eqn (15a)), whereas electron transfer will result in the oxidation or reduction of the photocatalyst (with corresponding reduction or oxidation of the substrate, eqn (15b) and (c)). Direct detection of one (or more) of these products is the gold standard by which mechanistic pathways in these reactions must be established.

Time-resolved absorption spectroscopy, also known as transient absorption (TA), is a very useful tool in these cases.

¶¶ The above discussion may suggest that Stern–Volmer quenching studies can only be done with an emissive donor (such as $[Ru(bpy)_3]^{2+}$); however, if the photocatalyst does not emit (or if its emission is too weak) Stern–Volmer quenching studies can be carried out using transient absorption spectroscopy; the data analysis is done in the same way as described for time-resolved emission.

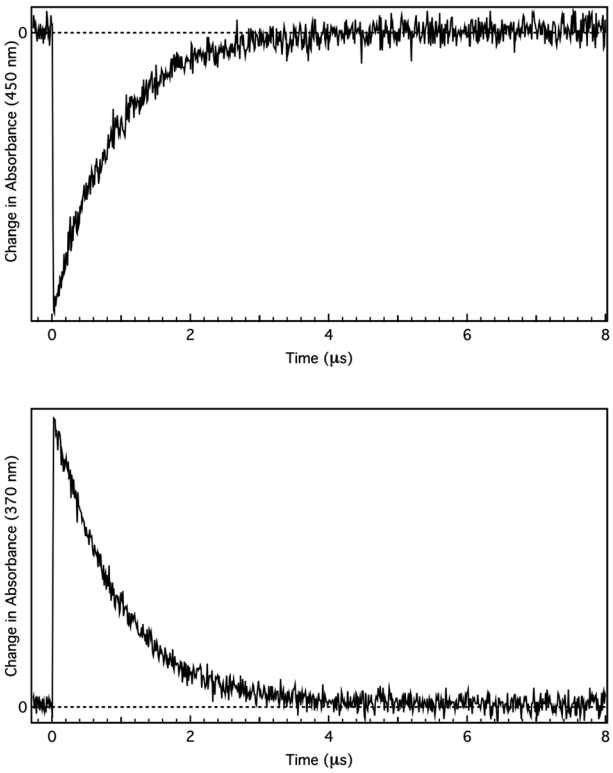

Fig. 7 Kinetic traces for $[Ru(bpy)_3]^{2+}$ following MLCT excitation at 475 nm in acetonitrile solution. Top: λ_{probe} = 450 nm. The negative signal (*i.e.*, "bleach") is due to the presence of Ru^{III} (or, conversely, the loss of Ru^{II}) in the excited state relative to the ground state. Bottom: λ_{probe} = 370 nm. This positive feature arises due to the presence of the reduced ligand in the MLCT excited state.

This technique uses a laser pulse to excite the sample and a white light source to probe the absorption of the transient species formed due to excitation. In many ways, one can think of transient absorption spectroscopy as taking a UV-Vis spectrum of an excited state, using the absorption of the ground state as the blank. The TA signal, then, is the change in absorbance of the sample before and after excitation. This renders the technique more versatile than time-resolved emission, because non-emissive molecules can be studied as well. Depending on the instrumentation available, difference spectra can be acquired at single wavelengths (yielding kinetic traces, as shown in Fig. 7) or a full spectrum can be obtained.

For a TA experiment, an expression derived from Beer's law can be written, as shown in eqn (31),

$$\Delta A = \Delta\varepsilon \cdot b \cdot [GS] \cdot \eta^{ex} \quad (31)$$

where ΔA is the change in absorbance before and after excitation (*i.e.*, excited state minus ground state), $\Delta\varepsilon$ is the change in molar absorptivity (the difference between the ground state and the excited state), b is the optical path length, [GS] is the concentration of the ground state (*i.e.*, the concentration of the sample) and η^{ex} is the fraction of molecules that are excited from the ground state to the excited state ($0 < \eta^{ex} < 1$). For a given experiment, b and [GS] are constant. η^{ex} depends on,

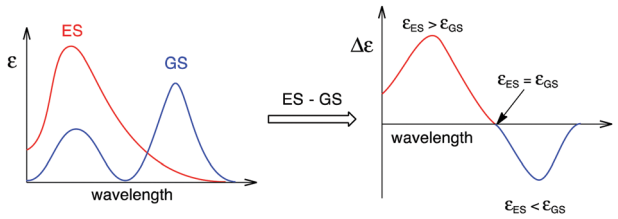

Scheme 9 Left: Schematic absorption spectra of the ground and excited states. Right: Schematic representation of a transient absorption plot. The positive feature is shown in red, while the bleach is in blue.

among other factors, the cross-section between the pump and probe beams, but remains constant as long as the experimental conditions are not changed. When that is the case, any changes in the sign of ΔA are a direct reflection of the changes in $\Delta\varepsilon$.

Scheme 9 presents a qualitative way to view the type of information obtained in a TA experiment. If at a certain wavelength the excited state absorbs more strongly than the ground state, a positive feature is observed. Conversely, if the ground state absorbs more than the excited state, a negative feature (''bleach'') is obtained. The wavelengths at which the excited and ground states have the same molar absorptivity are called isosbestic points.

In the case of the MLCT excited state of $[Ru(bpy)_3]^{2+}$, the main diagnostic feature for the oxidized species is a bleach centered around 450 nm; this signal reflects the loss of Ru(II) in the excited state relative to the ground state (or the presence of Ru(III), depending how you look at it).[39] In contrast, the absorption centered around 370 nm indicates the presence of a bpy radical anion, and corresponds to the ''reduced'' portion of the excited state.[39] Kinetic traces for both of these features in the absence of any quencher are shown in Fig. 7. It should be noted that as the excited molecules relax back to the ground state, both of these decay and the kinetic trace goes back to zero, indicative of ground-state recovery.

Now let us consider what happens to the TA traces upon adding a quencher. To illustrate the different scenarios, several simulated TA traces are shown in Fig. 8. For the unquenched photocatalyst, a lifetime of 700 ns was used. To make comparisons easier, a lifetime of 300 ns was assumed for the quenched photocatalyst, regardless of the reaction taking place. Upon photoexcitation, the excited state, $[Ru^{III}(bpy^{-})(bpy)_2]^{2+*}$, is formed, leading to a positive feature at 370 nm (due to bpy^{-}) and a bleach at 450 nm (diagnostic for Ru^{III}). If no quencher is present, both traces go back to zero with the same rate constant (*i.e.*, $1.4 \times 10^7\ s^{-1}$).

In the presence of an energy acceptor, the product of the quenching reaction is $[Ru(bpy)_3]^{2+}$, the same species present before excitation (see eqn (15a)), so both the Ru^{III} and the $bpy^{\bullet -}$ signals are lost at the same time, with an observed rate constant, k_{obs}, that is larger than k_0 (see eqn (25) and (26)). This illustrates what amounts to the most critical diagnostic for an energy transfer mechanism, namely the simultaneous, kinetically indistinguishable loss of both the $bpy^{\bullet -}$ and Ru^{III} species. This occurs because both of these components comprise the reactive excited state, and therefore both are lost in an energy transfer process that returns the chromophore to the ground state.

In the case of an electron transfer, the products of the quenching reaction are chemically distinct from $[Ru(bpy)_3]^{2+}$ (see eqn (15b) and (c)). In the case of a reductive quenching, the excited photocatalyst is reduced to $[Ru(bpy^{\bullet -})(bpy)_2]^{+}$ due to its reaction with the substrate. This has two consequences: (1) persistence of the

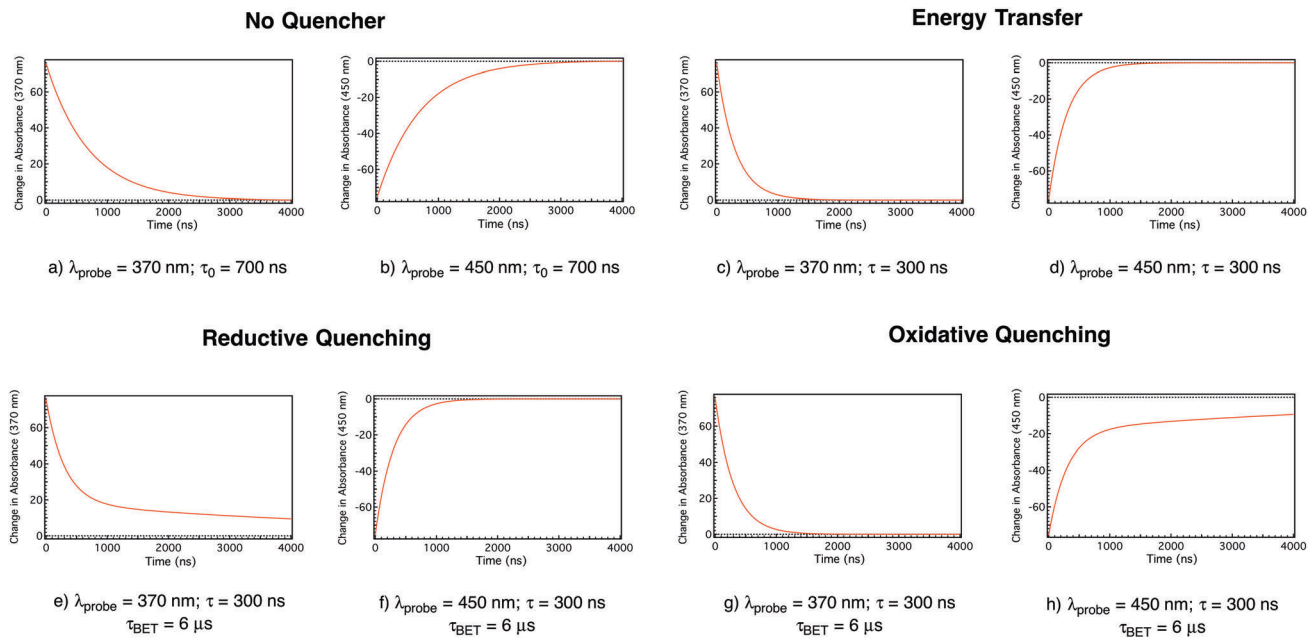

Fig. 8 Simulated TA traces for $[Ru(bpy)_3]^{2+}$ following MLCT excitation with no quencher (a and b), in the presence of an energy transfer acceptor (c and d); in the presence of an electron donor (e and f); and in the presence of an electron acceptor (g and h).

absorption feature at 370 nm, concomitant with (2) a partial recovery of the bleach at 450 nm. The recovery of the bleach signal is only partial because, although reduction converts the Ru^{III} species present in the excited state to Ru^{II}, the ground-state MLCT absorption has three contributions (*i.e.*, MLCT transitions to each of the three bpy ligands): the product of reductive quenching therefore only recovers ~2/3 of its original intensity due to the persistence of $bpy^{\bullet -}$. This situation is illustrated in Fig. 8e. Oxidative quenching, on the other hand, results in the formation of $[Ru^{III}(bpy)_3]^{3+}$. This will result in the mirror image of the observables just described for reductive quenching wherein the bleach persists concomitant with the loss of the $bpy^{\bullet -}$ signal at 370 nm.

Given these descriptions, the key qualitative differences between an electron and energy transfer quenching process lie in the wavelength dependence of the observed kinetics: for energy transfer one observes wavelength independent kinetics, whereas electron transfer results in qualitatively different kinetic traces depending on probe wavelength and the nature (*i.e.*, oxidative or reductive) of the reaction.

It should be noted that we have focused on the spectroscopic signatures of the excited state of $[Ru(bpy)_3]^{2+}$ for this discussion because its reduced and oxidized forms have easily distinguishable electronic absorption spectra. This does not exclude the possibility of monitoring one of the substrates *via* TA spectroscopy provided that its reduced and oxidized forms absorb light in different ways so that their spectra can be clearly identified (*e.g.*, through the use of spectroelectrochemical measurements) and/or distinguished.

8. Designing photocatalysts: $[Ru(bpy)_3]^{2+}$ as a starting point

As was mentioned in the introduction, there are some desirable characteristics for a photocatalyst:

(1) Strong absorption of light over a spectral region distinct from the substrates of interest.

(2) Stability in solution.

(3) Excited-state lifetime in the nanosecond to microsecond range.

(4) Reversible redox behavior (with values for ground- and excited-state redox potentials defined by the reaction of interest).

(5) Ease of synthesis and tunability of ground- and excited-state properties.

We have used $[Ru(bpy)_3]^{2+}$ as a convenient example to discuss the relevant properties of a photocatalyst. Scheme 10 illustrates both types of catalytic cycles that $[Ru(bpy)_3]^{2+}$ can take part in, where D and A represent a generic electron donor and acceptor, respectively.

Using the reductive quenching cycle as an example, both the initial reduction of the excited state (eqn (32)) and its subsequent oxidation (eqn (33)) must be favorable in order to complete the catalytic cycle.

$$[Ru^{III}(bpy^{\bullet -})(bpy)_2]^{2+*} + D \rightarrow [Ru^{II}(bpy^{\bullet -})(bpy)_2]^{+} + D^{+} \quad (32)$$

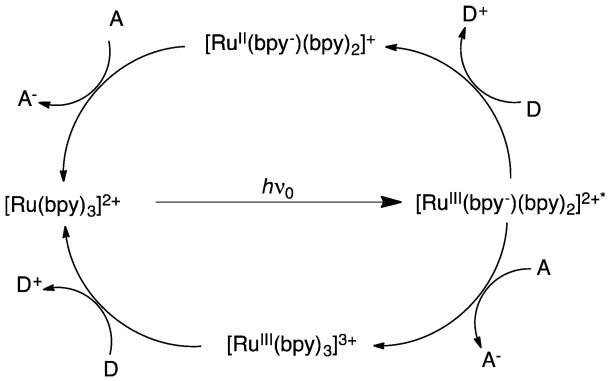

Scheme 10 Generic catalytic cycles *via* reductive quenching (top half) and oxidative quenching (bottom half).

$$[Ru^{II}(bpy^{\bullet -})(bpy)_2]^{+} + A \rightarrow [Ru^{II}(bpy)_3]^{2+} + A^{-} \quad (33)$$

The exothermicity of these steps can be evaluated in a straightforward manner as specified in eqn (34) and (35):

$$\Delta E_{M/D} = E(M^{*}/M^{+}) - E(D^{+}/D) \quad (34)$$

$$\Delta E_{A/L} = E(A/A^{-}) - E(L/L^{-}) \quad (35)$$

It is easy to see that the identities of A/A^{-} and D/D^{+} (and therefore their redox potentials) determine which compounds can act as photocatalysts for a given reaction. The redox potentials of the A/A^{-} and D^{+}/D couples can be determined using electrochemistry. If either the donor or the acceptor is formed *in situ* during the reaction, the determination of the thermodynamic viability of the desired reaction becomes extremely difficult (if not impossible) to assess *a priori*. In these situations, empirical results may have to suffice.

It was mentioned before that the redox activity of $[Ru(bpy)_3]^{2+}$ is enhanced in the excited state relative to the ground state: this circumstance arises due to the combined effects of charge separation (thereby creating chemical potential) as well as the increase in internal energy of the molecule due to the absorption of light.‖‖ Whether a compound is a suitable photocatalyst for a given reaction therefore depends on the redox potentials of both the ground and excited states. Excited-state redox potentials cannot be directly measured, but can be calculated using the redox potentials for the ground state and the energy of the excited state. The relationship between these quantities is presented in Scheme 11. Assuming that the all the excited state energy is available as free energy (*i.e.*, the entropic contribution is neglected),[40] the excited state redox potentials can be calculated using eqn (36) and (37).[15,28]

$$E(M^{+}/M^{*}) = E(M^{+}/M) - E_0 \quad (36)$$

$$E(L^{*}/L^{-}) = E(L/L^{-}) + E_0 \quad (37)$$

‖‖ Keep in mind that 600 nm light corresponds to ~16 000 cm^{-1}, or the equivalent of roughly 45 kcal mol^{-1}.

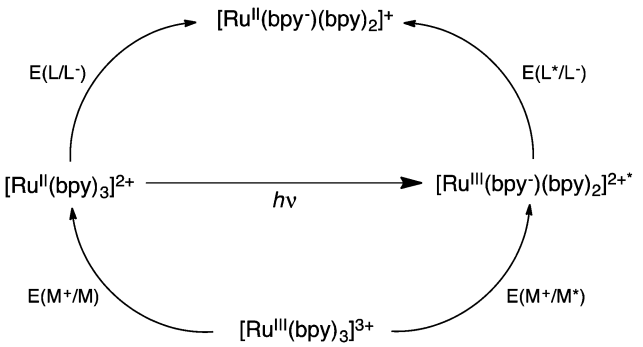

Scheme 11 Thermodynamic cycle relating the excited and ground state potentials.

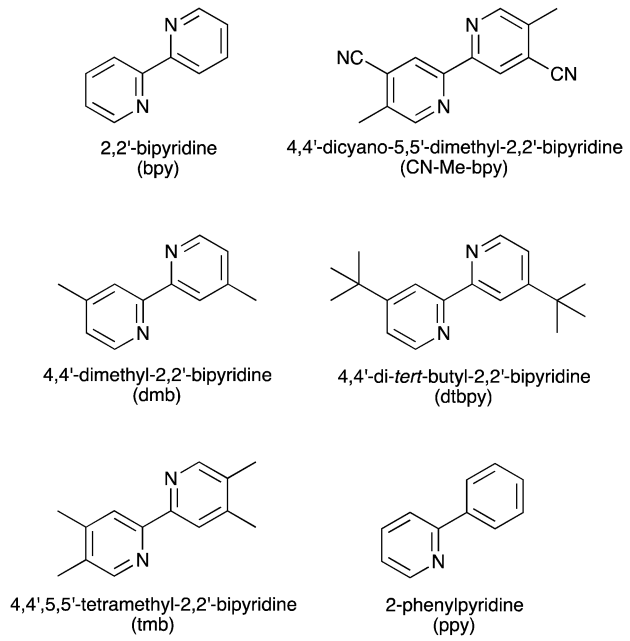

Fig. 9 Molecular structures of the ligands included in the compounds presented on Table 1.

We have stated that an advantage of transition metal polypyridyl complexes is that their properties can be modified by altering the ligands coordinated to the metal center or by changing the metal itself. To illustrate this point, Table 1 summarizes the ground- and excited-state redox potentials of some Ru(II) and Ir(III) coordination compounds (note that not all of these have been used as photoredox catalysts). The corresponding ligands are shown in Fig. 9. As a general rule, the presence of electron-withdrawing substituents on the ligands makes them easier to reduce while the metal becomes harder to oxidize (*e.g.*, compare $[Ru(bpy)_3]^{2+}$ and $[Ru(CN\text{-}Me\text{-}bpy)_3]^{2+}$). The opposite is true when the ligands have electron-donating substituents (*e.g.*, $[Ru(dmb)_3]^{2+}$ and $[Ru(tmb)_3]^{2+}$). Comparing Ru(II) and Ir(III), the latter is less electron rich, which makes it harder to oxidize (*e.g.*, $[Ru(bpy)_3]^{2+}$ *versus* $[Ir(bpy)_3]^{3+}$) while at the same time making the bpy ligand easier to reduce. In the case of the cyclometalated compounds (those containing 2-phenylpyridine) the reduction of ppy is much less favorable than that of bpy, because ppy is formally an anionic ligand. These anionic ligands also make the metal easier to oxidize.

Since modifying the ligands and/or the metal center modulates the ground state redox potentials of the compound, it comes as no surprise that the electronic absorption and emission spectra are also affected. This in turn implies that the redox potentials of the excited state change as well. Generally speaking, changes in the ligands (such as the presence of substituents) tend to have a greater impact on the electrochemical properties of the compound than on E_0.[18,40] It should also be noted that these changes in the energetics of the ground and excited states also impact excited-state lifetimes. However, in most cases the changes in lifetimes remain within a temporal window to retain their utility in bimolecular reactions.

The degree of redox tunability afforded by the relatively minor compositional variations reflected in Table 1 represents a powerful tool for applications in photoredox catalysis. If the mechanism of a photoredox catalyzed reaction is known, and the relevant redox potentials for the intervening substrates have been measured, it is possible, at least in principle, to design the best-suited photocatalyst for that system.

It must be noted that, with the exception of the neutral $Ir(ppy)_3$, the solubility of these coordination compounds can be modulated quite substantially by changing the counterion. For example, chloride (Cl^-) or nitrate (NO_3^-) salts of many metal polypyridyl complexes are soluble in water, whereas using hexafluorophosphate (PF_6^-) or tetraphenylborate (BPh_4^-) enhances their solubility in organic solvents such as acetone,

Table 1 Ground- and excited-state properties of Ru(II) and Ir(III) coordination compounds

Compound	$E(M^+/M)^a$ (V)	$E(L/L^-)^a$ (V)	$E(M^+/M^*)$ (V)	$E(L^*/L^-)$ (V)	λ_{abs} (nm)	λ_{em} (nm)	τ (μs)
$[Ru(bpy)_3]^{2+}$	1.31	−1.30	−0.72	0.73	452	618	0.95
$[Ru(dmb)_3]^{2+}$	1.14	−1.43	−0.85	0.56	458	625	0.93
$[Ru(tmb)_3]^{2+}$	1.04	−1.61	−1.01	0.44	449	605	0.49
$[Ru(CN\text{-}Me\text{-}bpy)_3]^{2+}$ [49]	1.69	−0.85	−0.29	1.14	458	626	3.50
$[Ir(bpy)_3]^{3+}$ [4,5]	1.93	−1.00	−0.88	1.81	344[a]	441[a]	2.40[a]
$[Ir(ppy)_2(dtbpy)]^+$	1.29	−1.43	−0.84	0.70	410[a]	585[a]	0.62[a]
$[Ir(ppy)_2(bpy)]^+$ [50]	1.27	−1.38	−0.79	0.68	420	602	0.28
fac-$Ir(ppy)_3$ [3]	0.77	−2.19	−1.73	0.31	375	494[b]	1.90

All redox potentials reported *vs.* SCE. Measurements were performed in acetonitrile at room temperature unless otherwise noted.[a] Measured in methanol. [b] Measured in 1 : 1 ethanol/methanol glass at 77 K.

methanol or acetonitrile. If low polarity solvents are necessary, tetrakis[(3,5-trifluoromethyl)phenyl]borate ($[BAr^F_4]^-$) can in some cases facilitate dissolution of even 2 : 1 salts into solvents like diethyl ether or decanol. Thanks to this added degree of flexibility, the choice of the solvent can be based on the organic transformation under study, without necessarily being limited in terms of which photocatalyst can be used. It is, however, important to remember that the solvent may affect the redox and spectroscopic properties of coordination compounds.

A more extensive survey of Ru(II) and Ir(III) coordination compounds is beyond the scope of this review; however, this information is available elsewhere.[2,3]

Finally, it is important to bear in mind that the above discussion focused on the thermodynamics of photoinduced electron transfer. As was discussed in Section 5.2, the rate of electron transfer depends not only on the driving force for the process, but also on the reorganization energy and the electronic coupling between the donor and the acceptor (see eqn (22)). This means that, even if an electron transfer reaction is thermodynamically viable, its kinetics may not be favorable. Consequently, the strategies outlined in this section must be taken as a starting point, aimed to reduce the guesswork in the choice of a photocatalyst. Once a sound candidate has been identified, its utility for a given reaction must still be experimentally assessed.

9. Moving away from Ru and Ir: first-row transition metals and organic dyes

As was stated in the introduction, iridium- and ruthenium-based photocatalysts have been widely used in the past decade.[11] Despite their many successful applications, they do have some drawbacks that are worth noting. First, iridium and ruthenium are among the rarest elements on Earth, which not only makes their compounds very expensive, but potentially limits the scalability of the reactions they catalyze. The toxicity associated with these metals, even in small quantities, can also be an issue of concern in certain circumstances.

One possibility is to replace Ru(II) and Ir(III) for their first-row congeners, *e.g.*, Fe(II) and Co(III). $[Fe(bpy)_3]^{2+}$ for example, has recently been reported in the context of photoredox catalysis.[41] The mechanism of action in this case is unlikely to proceed in a manner similar to the Ru and Ir-based catalysts discussed thus far due to the fact that the ^{3}MLCT of Fe(II) polypyridyl compounds relaxes to metal-centered (d–d) excited state(s) in less than 100 fs.[42] This corresponds to a rate constant that is orders of magnitude faster than the time scale for diffusion. This is likely to be a problem for a significant fraction of charge-transfer complexes of the first transition series with the notable exception of Cu(I). Because of its d^{10} valence configuration, the lowest-energy excited state of polypyridyl complexes of Cu(I) is MLCT in nature. This results in photophysical properties of such compounds that are very reminiscent of Ru(II) and Ir(III)-based photocatalysts. Several examples of Cu(I) compounds being used as photoredox catalysts have been reported; MacMillan and co-workers have reviewed many of these.[11]

The preceding discussion underscores the fact that the development of first-row transition-metal-based photoredox catalysts is not without challenges. Organic dyes offer considerable promise as an alternative to the metal-based approaches that have largely dominated the field. For example, Fukuzumi and co-workers reported several examples of oxidations photocatalyzed by 10-methylacridinium ion.[43,44] Since then, interest in the use of organic chromophores for photoredox catalysis has grown steadily; Romero and Nicewicz have recently published an excellent overview of this work.[12]

Going back to our "wish list" for photocatalysts, it is no surprise that organic dyes have been the main focus of these studies. These compounds are intensely colored and very stable in solution. In addition, their excited-state redox potentials are comparable to those of transition-metal-based photocatalysts.[45] Many organic dyes can be easily prepared and are amenable to synthetic modifications, which could make them very versatile photo-reagents. Xanthene dyes are an excellent example along these lines. Most of the concepts and methodologies discussed in this article apply equally well to organometallic and purely organic photocatalysts. It is worth noting that an important difference between transition-metal compounds and organic dyes is the nature of their reactive excited states: as was previously discussed, iridium and ruthenium photocatalysts owe their catalytic activity in large part to a metal-to-ligand charge transfer state, whereas for most organic dyes the reactive triplet state is not characterized by charge separation.[46] As a consequence, not all of these dyes can engage in both oxidative and reductive quenching, which can limit their applicability in certain catalytic cycles. That said, there are examples where bimodal reactivity is readily accessible. Eosin Y, arguably the organic dye most used as a photocatalyst so far,[47] can act both as a reductant and an oxidant in its excited state.[45] Very recent work by Miyake and co-workers[48] is an excellent example of some of the exciting opportunities that are possible using organic photoredox catalysts.

10. Conclusions

Over the last decade, photoredox catalysis has been a transformative force in synthetic organic chemistry. Despite the intense research in this area, oftentimes photocatalysts are chosen by trial-and-error rather than systematically considering their properties and how they relate to the reaction of interest. This is perfectly understandable given that, historically, the synthetic organic community had little in common with inorganic photophysics (and, to be sure, the converse is just as true). Photoredox catalysis represents an opportunity to bridge this divide to pursue chemistry that can become more than the sum of its parts; it can be argued that this is already happening in research groups around the world.

Our goal with this review has been to provide some relevant background in the fundamentals of inorganic photophysics

and photochemistry as it pertains to its application in photoredox catalysis, as well as survey the tools that have been developed over the years that allow for the systematic study of excited-state chemistry, with a particular emphasis on their application to study the types of reactions of interest to the photoredox catalysis community. It is our hope that the content of this review will allow synthetic chemists to select (and ultimately design) photoredox catalysts tailored to the reactions of interest, and in so doing open up opportunities for developing new science at the interface of organic and inorganic chemistry.

Note added in proof

In the course of finalizing revisions to this Tutorial, the authors became aware of a special issue of Accounts of Chemical Research on Photoredox Catalysis in Organic Chemistry, (edited by Corey Stephenson and Tehshik Yoon) that is currently in process. The reader is referred to this on-line issue for the latest in this rapidly developing field.

Commonly used symbols and abbreviations

MLCT	Metal-to-ligand charge transfer
IL	Intraligand transition
LF	Ligand-field transition
k_{isc}	Rate constant for intersystem crossing
k_r	Rate constant for radiative decay
k_{nr}	Rate constant for non-radiative decay
E_0	Zero-point energy of the ^{3}MLCT excited state
Φ	Radiative quantum yield
k_0	Intrinsic (*i.e.*, no quencher) rate constant for excited-state decay
τ	Lifetime (= k^{-1}, where k is the rate constant)
k_{obs}	Observed rate constant
k_{EnT}	Rate constant for energy transfer
FRET	Fluorescence resonant (*i.e.*, Förster) energy transfer
k_{FRET}	Rate constant for fluorescence resonant energy transfer
k_{DET}	Rate constant for Dexter energy transfer
k_{ET}	Rate constant for electron transfer
k_q	Rate constant for quenching
K_D	Equilibrium constant for dynamic quenching
K_S	Equilibrium constant for static quenching
TA	Transient absorption
GS	Ground state
ES	Excited state
SCE	Standard calomel electrode

Acknowledgements

The authors would like to thank Professors David W. C. MacMillan and David A. Nicewicz for many fruitful discussions, as well as Dr Catherine E. McCusker for her efforts in the initial stages of our work on photoredox catalysis. Finally, although this review was not specifically the result of any external funding, the Solar Photochemistry Program within the Basic Energy Sciences branch of the Office of Science at the U.S. Department of Energy, as well as the Division of Chemistry within the Mathematical and Physical Sciences Directorate of the National Science Foundation have been generously supportive of our work on the photophysics of inorganic compounds.

References

1 F. E. Lytle and D. M. Hercules, *J. Am. Chem. Soc.*, 1969, **91**, 253–257.
2 A. Juris, V. Balzani, F. Barigelletti, S. Campagna, P. Belser and A. von Zelewsky, *Coord. Chem. Rev.*, 1988, **84**, 85–277.
3 L. Flamigni, A. Barbieri, C. Sabatini, B. Ventura and F. Barigelletti, *Top. Curr. Chem.*, 2007, **281**, 143–203.
4 I. M. Dixon, J.-P. Collin, J.-P. Sauvage, L. Flamigni, S. Encinas and F. Barigelletti, *Chem. Soc. Rev.*, 2000, **29**, 385–391.
5 V. Balzani, F. Bolletta, M. Gandolfi and M. Maestri, *Top. Curr. Chem.*, 1978, **75**, 1–64.
6 D. M. Hedstrand, W. H. Kruizinga and R. M. Kellogg, *Tetrahedron Lett.*, 1978, **19**, 1255–1258.
7 H. Cano-Yelo and A. Deronzier, *J. Chem. Soc., Perkin Trans.* 2, 1984, 1093–1098.
8 G. Pandey, G. Kumaraswamy and A. Krishna, *Tetrahedron Lett.*, 1987, **28**, 2649–2652.
9 D. A. Nicewicz and D. W. C. MacMillan, *Science*, 2008, **322**, 77–80.
10 M. A. Ischay, M. E. Anzovino, J. Du and T. P. Yoon, *J. Am. Chem. Soc.*, 2008, **130**, 12886–12887.
11 C. K. Prier, D. A. Rankic and D. W. C. MacMillan, *Chem. Rev.*, 2013, **113**, 5322–5363.
12 N. A. Romero and D. A. Nicewicz, *Chem. Rev.*, 2016, **116**, 10075–10166.
13 S. Maity, M. Zhu, R. S. Shinabery and N. Zheng, *Angew. Chem., Int. Ed.*, 2012, **51**, 222–226.
14 H. Cano-Yelo and A. Deronzier, *J. Photochem.*, 1987, **37**, 315–321.
15 D. Rehm and A. Weller, *Isr. J. Chem.*, 1970, **8**, 259–271.
16 L. Arnaut, S. Formosinho and H. Burrows, *Chemical Kinetics. From Molecular Structure to Chemical Reactivity.*, Elsevier, Amsterdam, 2007.
17 N. Sutin and C. Creutz, *Pure Appl. Chem.*, 1980, **52**, 2717–2738.
18 C. T. Lin, W. Bottcher, M. Chou, C. Creutz and N. Sutin, *J. Am. Chem. Soc.*, 1976, **98**, 6536–6544.
19 N. Sutin and C. Creutz, *Adv. Chem. Ser.*, 1978, **168**, 1–27.
20 R. S. Drago, *Physical Methods for Chemists*, Saunders College Pub, Philadelphia, 1992.
21 A. A. Vlcek, E. S. Dodsworth, W. J. Pietro and A. B. P. Lever, *Inorg. Chem.*, 1995, **34**, 1906–1913.
22 N. H. Damrauer, G. Cerullo, A. Yeh, T. R. Boussie, C. V Shank and J. K. McCusker, *Science*, 1997, **275**, 54–57.

23 J. P. Claude and T. J. Meyer, *J. Phys. Chem.*, 1995, **99**, 51–54.
24 The spectrum should be corrected according to Parker and Rees when converting from wavelength to energy units. For further details, see: C. A. Parker and W. T. Rees, *Analyst*, 1960, **85**, 587–600.
25 U. Resch-Genger and K. Rurack, *Pure Appl. Chem.*, 2013, **85**, 2005–2013.
26 K. Suzuki, A. Kobayashi, S. Kaneko, K. Takehira, T. Yoshihara, H. Ishida, Y. Shiina, S. Oishi and S. Tobita, *Phys. Chem. Chem. Phys.*, 2009, **11**, 9850–9860.
27 J. R. Lakowicz, *Principles of Fluorescence Spectroscopy*, Springer US, Boston, 3rd edn, 2006.
28 C. Creutz and N. Sutin, *Inorg. Chem.*, 1976, **15**, 496–499.
29 T. Förster, *Discuss. Faraday Soc.*, 1959, **27**, 7–17.
30 H. Sahoo, *J. Photochem. Photobiol., C*, 2011, **12**, 20–30.
31 G. D. Scholes, *Annu. Rev. Phys. Chem.*, 2003, **54**, 57–87.
32 D. L. Dexter, *J. Chem. Phys.*, 1953, **21**, 836–850.
33 F. Scandola, M. T. Indelli, C. Chiorboli and C. A. Bignozzi, *Top. Curr. Chem.*, 1990, **158**, 73–149.
34 B. Brunschwig and N. Sutin, *J. Am. Chem. Soc.*, 1978, **100**, 7568–7577.
35 J. N. Demas, E. W. Harris and R. P. McBride, *J. Am. Chem. Soc.*, 1977, **99**, 3547–3551.
36 F. Barigelletti and L. Flamigni, *Chem. Soc. Rev.*, 2000, **29**, 1–12.
37 R. A. Marcus, *Angew. Chem., Int. Ed. Engl.*, 1993, **32**, 1111–1121.
38 F. Scandola and V. Balzani, *J. Chem. Educ.*, 1983, **60**, 814–823.
39 A. M. Brown, C. E. McCusker and J. K. McCusker, *Dalton Trans.*, 2014, **43**, 17635–17646.
40 V. Balzani, F. Bolletta, F. Scandola and R. Ballardini, *Pure Appl. Chem.*, 1979, **51**, 299–311.
41 A. Gualandi, M. Marchini, L. Mengozzi, M. Natali, M. Lucarini, P. Ceroni and P. G. Cozzi, *ACS Catal.*, 2015, **5**, 5927–5931.
42 E. A. Juban, A. L. Smeigh, J. E. Monat and J. K. McCusker, *Coord. Chem. Rev.*, 2006, **250**, 1783–1791.
43 K. Ohkubo and S. Fukuzumi, *Org. Lett.*, 2000, **2**, 3647–3650.
44 K. Suga, K. Ohkubo and S. Fukuzumi, *J. Phys. Chem. A*, 2003, **107**, 4339–4346.
45 D. Ravelli and M. Fagnoni, *ChemCatChem*, 2012, **4**, 169–171.
46 U. Resch-Genger, M. Grabolle, S. Cavaliere-Jaricot, R. Nitschke and T. Nann, *Nat. Methods*, 2008, **5**, 763–775.
47 D. P. Hari and B. König, *Chem. Commun.*, 2014, **50**, 6688–6699.
48 J. C. Theriot, C.-H. Lim, H. Yang, M. D. Ryan, C. B. Musgrave and G. M. Miyake, *Science*, 2016, **352**, 1082–1086.
49 C. E. McCusker and J. K. McCusker, *Inorg. Chem.*, 2011, **50**, 1656–1669.
50 S. Ladouceur, D. Fortin and E. Zysman-Colman, *Inorg. Chem.*, 2011, **50**, 11514–11526.

